Molecular structure, spectroscopic investigation (FT-IR, ^{1}H NMR, ^{13}C NMR and Mass) and quantum chemical calculations of Ruthenium (II) complex of isoniazid ligand

Rupal Yadav & R M Naik*

Department of Chemistry, University of Lucknow, Lucknow 226 007, India

The present study aims at the synthesis of $[Ru(CN)_5INH]^{3-}$ complex by substitution of cyanide ion in $[Ru(CN)_5H_2O]^{3-}$ anion by isoniazid (pyridine-4- carboxylic acid hydrazide) (INH) ligand. The reaction has been monitored spectrophotometrically in aqueous medium, by measuring an increase in absorbance at 500 nm (λmax of the light yellow coloured complex), which corresponds to the metal to ligand charge transfer (MLCT) transition, due to the formation of the final substituted complex $[Ru(CN)_5INH]^{3-}$. The synthesized complex $[Ru(CN)_5INH]^{3-}$ has been characterized by ^{1}H and ^{13}C nuclear magnetic resonance, infrared and mass spectral analysis. Quantum mechanical calculations have been performed at DFT level using Becke3-Lee-Yang-Parr (B3LYP) with LanL2DZ basis set. The experimental spectroscopic data has been found to be in good agreement with the calculated results. The Mulliken population analysis on atomic charges, electric dipole moment, polarizability and first order hyperpolarizability values have been evaluated along with hyper conjugative interactions which have been studied with the help of natural bond orbital analysis. Thermodynamic properties like heat capacity, entropy and zero vibrational energy have been analysed at different temperatures.

Keywords: Isoniazid (INH), Natural bond orbital (NBO), Non linear optical (NLO), Reactivity descriptors

1 Introduction

Tuberculosis is a bacterial disease, caused by pathogen *Mycobacterium tuberculosis* (MTb), currently influences approximately one–third of the population worldwide[1]. Tuberculosis (TB) is one of the most prevalent infectious diseases common to mankind[2] and being compared with other diseases, it is found to be globally second biggest killer[3]. Its main symptom includes chronic body cough[4]. It has been pre-analysed that if new prevention methods against tuberculosis have not been employed, approximately one billion people would be newly reported[5], suffering from TB and 360 million deaths will happen between 2002 and 2020. This disease is alone responsible for more than two million deaths per year[6]. Although the incidence and mortality rate due to TB is decreasing but still 9 million new cases and 1.5 million deaths are reported in 2014 by World Health Organization (WHO) in 2015. Shorter treatment duration is needed to suppress the TB epidemic completely[7]. Isoniazid (INH), a prodrug, recommended by WHO, is used in the prevention and treatment of tuberculosis[8,9] (Fig. 1). It was first

synthesized[10] in 1912 and was found[11] to be effective against tuberculosis in 1951. Isoniazid is a first line drug, bio-activated by the bacterial anti-oxidant enzyme (KatG)[12] and penetrates the tubercle bacilli by passive diffusion[13]. In subsequent steps, it inhibits the biosynthesis of mycolic acid[14], which is a major component in cell wall of *Mycobacterium tuberculosis*. Rifampicin (RIF) and Isoniazid (INH) are considered as the most potent first-line drugs and resistance against these drugs is known as Multidrug Resistance (MDR)[15].

Due to its enormous medicinal applications, use of coordination compounds of iron and ruthenium has been enhancing against cancer, parasitosis and tuberculosis diseases[16]. In this respect, one of the methods used extensively for the treatment of the problems related with the chemotherapy of

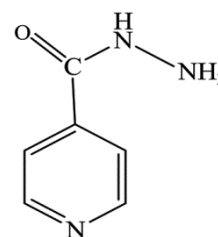
Fig. 1 – Structure of isoniazid.

*Corresponding author (E-mail: radheynaik@gmail.com)

tuberculosis is coordination of the prodrug with the metal complexes[17]. Ruthenium complexes have been proved quite beneficial in this respect due to their immense applications in field of synthetic and analytical chemistry[18]. The geometry, mainly exhibited by these complexes are pseudo-octahedral which display variable oxidation states[19] such as Ru(II), Ru(III) and Ru(IV). The ruthenium complexes also play an important role with polydentate ligands in catalytic reactions[20].

The substitutional behaviour of $[Ru(CN)_5H_2O]^{3-}$ ion was also made by Naik $et\ al.$[21] with naphthalene substituted ligands. The aquapentacyanoruthenate(II) ion easily loses a coordinated water molecule upon reaction with incoming or substituting ligand and subsequently forms highly stable nitrogen substituted complexes[21,22]. In the present paper, the emphasis is made to the synthesis and characterization of the complex, $[Ru(CN)_5INH]^{3-}$ as well as on its computational behaviour. The reaction between the $[Ru(CN)_5H_2O]^{3-}$ and isoniazid leads to the formation of a bright yellow colour complex, $[Ru(CN)_5(INH)]^{3-}$ (Fig. 2). The product composition has been found to be 1:1 by the mole ratio and slope ratio methods.

Characterization of complex is done with ^{1}H-NMR, ^{13}C-NMR, UV-Visible, FT-IR and mass spectroscopic analysis. The present study provides a complete description of molecular geometry, molecular vibrations and electronic features. DFT, a computational method, helps in the analysis of properties that are based on the determination of electron density. With the help of density functional theory (DFT) method, natural bond orbital (NBO), first order hyperpolarizability, electronic absorption spectra, global reactivity descriptors and thermodynamic properties were also evaluated, using basis set DFT/B3LYP/LanL2DZ.
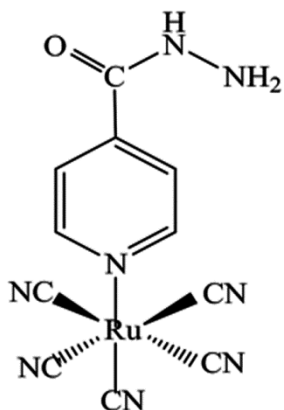

Fig. 2 – Structure of the product, $[Ru(CN)_5(INH)]^{3-}$.

2 Experimental

2.1 Materials and physical measurements

All chemicals used were of analytical reagent grade and were purchased from Alfa Aesar, Sigma–Aldrich and Merck. All the solutions were prepared, using deionised distilled water. All reagents were used without any further purification, unless otherwise specified.

Infrared (IR) spectrum was recorded on Perkin-Elmer Fourier transform infra-red spectrophotometer. Nuclear magnetic resonance spectra were recorded on Bruker DRX- 300 MHz instrument using TMS (0.0 ppm) as an internal reference and D_2O as a solvent. Elemental analysis was done using a Euro Vector E 3000 Elemental Analyser. The positive electron spray ionization (ESI) High resolution mass spectrometry of the compound was recorded by Agilent 6520(Q-TOF) mass spectrometer. A UV-Visible Double-Beam Spectrophotometer (systronic-2203) instrument, fitted with a cell compartment, was used for monitoring the progress of the reaction. Solutions were stored in dark to prevent photo decomposition. $NaClO_4$ (Merck) was used to maintain the ionic strength in the reaction mixture.

2.2 Synthesis of $[Ru(CN)_5INH]^{3-}$ complex

The aquapentacyanoruthenate(II) ion, $[Ru(CN)_5H_2O]^{3-}$ can be prepared in solution by dissolving 0.0468 g (0.1 mmol) of $K_4[Ru(CN)_6].3H_2O$ in 10 mL of deionised distilled water. Further, 0.137 g (1 mmol) of isoniazid was added to this solution. During the stirring of the mixture, 10 mL of Br_2 water (0.01 M Br_2, 0.1 M KBr) was added slowly[23]. The reaction of Br_2 with $[Ru(CN)_6]^{4-}$ is very rapid and generates the pale yellow colour solution of $[Ru(CN)_5H_2O]^{3-}$.

$$[Ru(CN)_6]^{4-} + Br_2 \xrightarrow{H_2O} [Ru(CN)_5H_2O]^{3-} + Br^- + BrCN$$
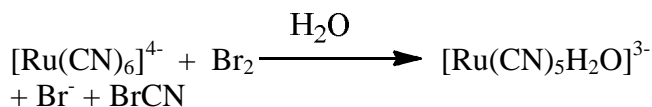
This pale yellow solution of $[Ru(CN)_5H_2O]^{3-}$ shows an absorption maximum at 310 nm with $\varepsilon = 1640 \pm 50$ $M^{-1}cm^{-1}$. It took approximately one hour for the reaction with isoniazid to be completed. As the reaction proceeds, the yellow colour of the solution intensifies. After completion of the reaction, the solution was chilled and product was precipitated by addition of cold acetone (Scheme 1). The reaction was analysed spectrophotometrically for completion. The formed complex (Fig. 2) was characterized by elemental analysis, UV-visible, IR and NMR spectroscopy.
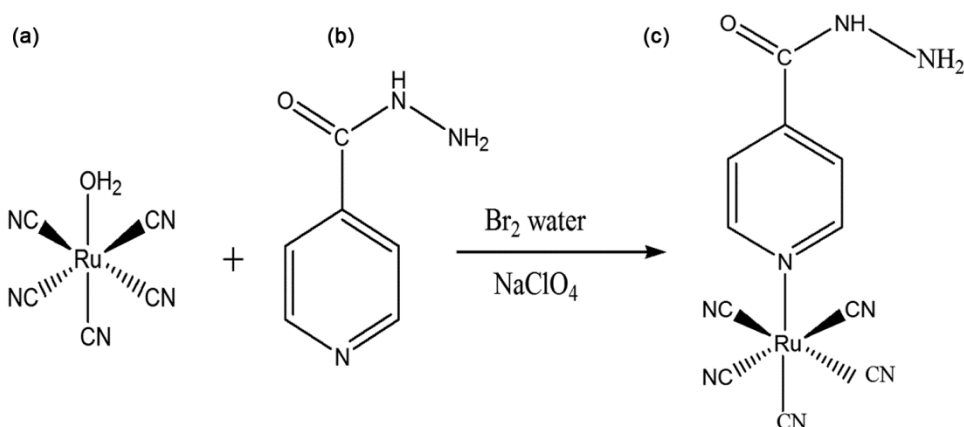
Scheme 1 – Synthesis of pentacyanopyridine-4-carbohydrazidoruthenate(II) ion ([Ru(CN)$_5$INH]$^{3-}$) complex.

2.2.1 Complex [Ru(CN)$_5$INH]$^{3-}$

Yield: 68 - 72%. (0.268gm); C$_{11}$H$_7$N$_8$ORu: Anal. Found: %C,35.87; %H,1.92; %N, 30.42, Calc.: %C,35.06; %H,1.88; %N, 30.16.IR (KBr) (cm^{-1}) ν_{max}: 3111.18 cm^{-1} (Asymmetric NH stretching); 3049.46 cm^{-1} (Symmetric NH stretching); 1635.64 cm^{-1} (C=O stretching); 3014.74 cm^{-1} (=C-H stretching); 2054.19 cm^{-1} (CN stretching); 1556.55 cm^{-1} (C=C stretching);^{1}H NMR (D$_2$O): δ = 8.62 ppm (d, 2H); 7.63ppm (d, 2H); ^{13}C NMR (D$_2$O): δ = 121.58 ppm, 121.92 ppm, 140.61 ppm, 149.43 ppm, 167.06 ppm; MS, m/z: 365.00.

2.3 Computational details

All quantum computations of synthesized complex were fully optimized with the help of density functional theory (DFT) method, using the B3LYP hybrid- exchange correlation functional of GAUSSIAN-09W and LanL2DZ basis set[24]. The optimized structure of ruthenium complex is shown in Fig. 3 along with numbering of atoms as ball and stick model. It has been proved earlier that at various levels this theory helps in producing very accurate geometric parameters for different organic molecules and at a very low computational cost[25]. Theoretically calculated vibrational wavenumbers were compared with experimentally observed FT-IR data. In order to discard the anharmonicity present in real system, calculated wavenumbers were scaled down using scaling factor[26] 0.9608. Values of polarizability (α_0) and first static hyperpolarizability (β_0) were calculated using the finite field perturbation method in vacuum[27]. Magnitude of mean first hyperpolarizability tensor was calculated by using x, y and z component from Gaussian output. Polarizability and total static hyperpolarizability values are obtained in atomic units so they have been converted in to electrostatic units
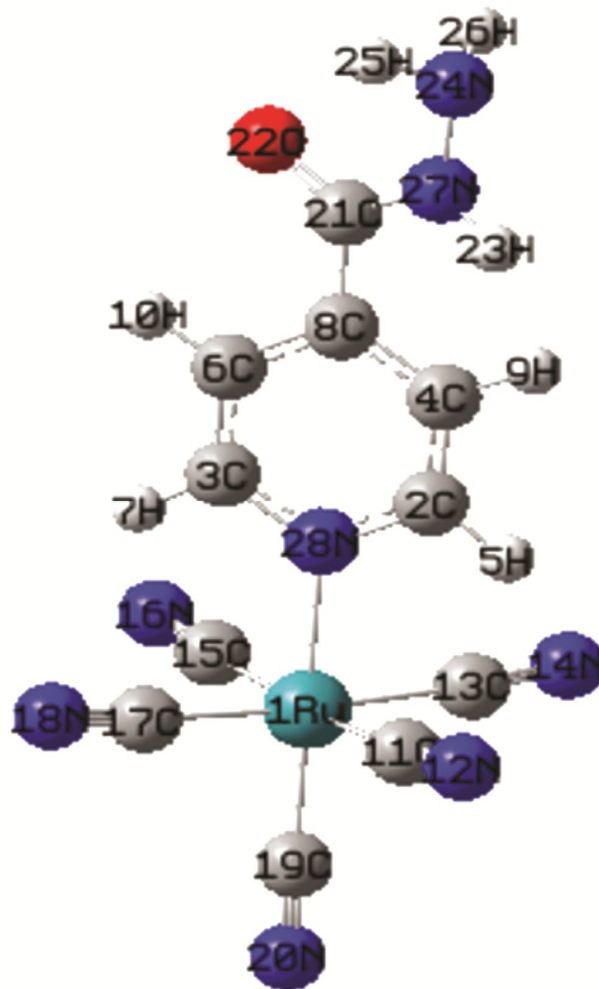

Fig. 3 – Optimized geometry of Ruthenium complex using B3LYP/LanL2DZ theory.

(esu) (α: 1a.u. = 0.1482 × 10^{-24}esu, β: 1a.u. = 8.6393 × 10^{-33}esu). Natural bond orbital (NBO)[28] analysis has been performed in order to gain information about the charge distribution within the molecule[29].

3. Results and Discussion

3.1 Vibrational spectral assignment

Theoretical vibrational analysis of the synthesized ruthenium metal complex has been performed, using DFT with basis set DFT/B3LYP/LanL2DZ. Experimental FT-IR spectra of synthesized ruthenium metal complex has been analysed within the experimental range 4000-450 cm^{-1}. Theoretical vibrational analysis suggests that given compound possess 28 atoms and 78 fundamental modes of vibration and belong to C_1 point group. The experimental and calculated vibrational wavenumbers and their respective vibrational assignments are given in Table 1. Experimental and theoretical FT-IR spectra are shown in Fig. 4. In order to remove discrepancy between observed and calculated vibrational wavenumbers, calculated wavenumbers are scaled down by using a scaling factor[30] 0.9608.

Table 1 – Experimental and theoretical vibrational wavenumbers (calculated at B3LYP/ LanL2DZ level) and their vibrational assignments: Wavenumbers (cm^{-1}) and intensity (Kmmol^{-1}).

Calculated		Obs	IR_{int}	Vibrational assignment (PED %)
Unscaled	Scaled			
409	392.9672		17.28433	τ(C3C6)(14.)
427	410.2616		10.67494	δ(C11N12)(25.)
436	418.9088		21.48792	δ(C17N18)(35.)
445	427.556		11.00163	(δoop-C19N20)(11.)
454	436.2032		17.71543	δ(C4C8C6)(26.)
517	496.7336		15.14149	(δoop– C13N14)(14.)
580	557.264		401.3199	(δoop– N27H23)(27.)
706	678.3248	675.09	16.23611	δ(C3N28H7)(28.)
715	686.972		71.72541	τ(C2H5)(23.)
841	808.0328	844.82	437.1667	δ(N24H25H26)(9.)
868	833.9744		78.02037	δ(C2C4)(26.)
895	859.916		82.08354	δ(C3C6)(29.)
904	868.5632		170.1972	δ(C6C8C4)(23.)
994	955.0352	995.27	4.666855	(δoop-C2H5)(32)
1021	980.9768		68.92996	(δoop-C3H7)(31)
1030	989.624		84.90773	δ(C6C3N28)(21)
1075	1032.86		16.37969	τ(C6H10)(85.)
1093	1050.154		48.96293	τ(C4H9)(85.)
1138	1093.39	1141.86	6.898999	δ(C3C6H10)(54)
1219	1171.215	1220.94	34.89472	(δoop-C4H9)(41)
1264	1214.451		113.2943	δ(C6C3H7)(35)
1309	1257.687		144.9297	δ(C2N28C3)(86)
1318	1266.334		667.7081	τ_S(N24H25)(26)
1327	1274.982	1334.74	526.3165	(δoop-N24H25)
1462	1404.69		53.16808	(δoop-C3H7)(36)
1489	1430.631	1411.89	617.4788	(δoop-N27H23)(39)
1525	1465.22		58.09036	δ(C4C2H5)(86)
1579	1517.103	1556.55	171.4232	δ(C4C8C6)(83)
1633	1568.986	1635.64	948.9469	ν(C21O22)(74)
1642	1577.634		470.4871	ν(C2C4)(78)
1723	1655.458	1668.43	56.77201	δ(N24H26)(68)
2083	2001.346	2054.19	43.68136	τ_{AS}(C15N16)(76)
2092	2009.994		237.4659	τ_{AS}(C13N14)(84)
2101	2018.641		37.8853	τ_{AS}(C11N12)(79)
3208	3082.246	3049.46	54.92866	ν(C4H9)(81)
3244	3116.835		3.640266	ν(C6H10)(76)

(*Contd.*)

Table 1 – Experimental and theoretical vibrational wavenumbers (calculated at B3LYP/ LanL2DZ level) and their vibrational assignments: Wavenumbers (cm^{-1}) and intensity (Kmmol^{-1}). (*Contd.*)

Calculated		Obs	IR_{int}	Vibrational assignment (PED %)
Unscaled	Scaled			
3271	3142.777		2.146965	ν(C2H5)(89)
3280	3151.424		10.9661	ν(C3H7)(88)
3298	3168.718	3111.18	1.02575	τ_S(N24H26)(84)
3577	3436.782	3302.13	1.478295	τ_{AS}(N24H25)(87)
3676	3531.901		71.74034	ν(N27H23)(92)

ν– stretching, δsc – scissoring, ρ – rocking, ω – wagging, δ-deformation, δs – symmetric deformation, δas – asymmetric deformation, τ – torsion.
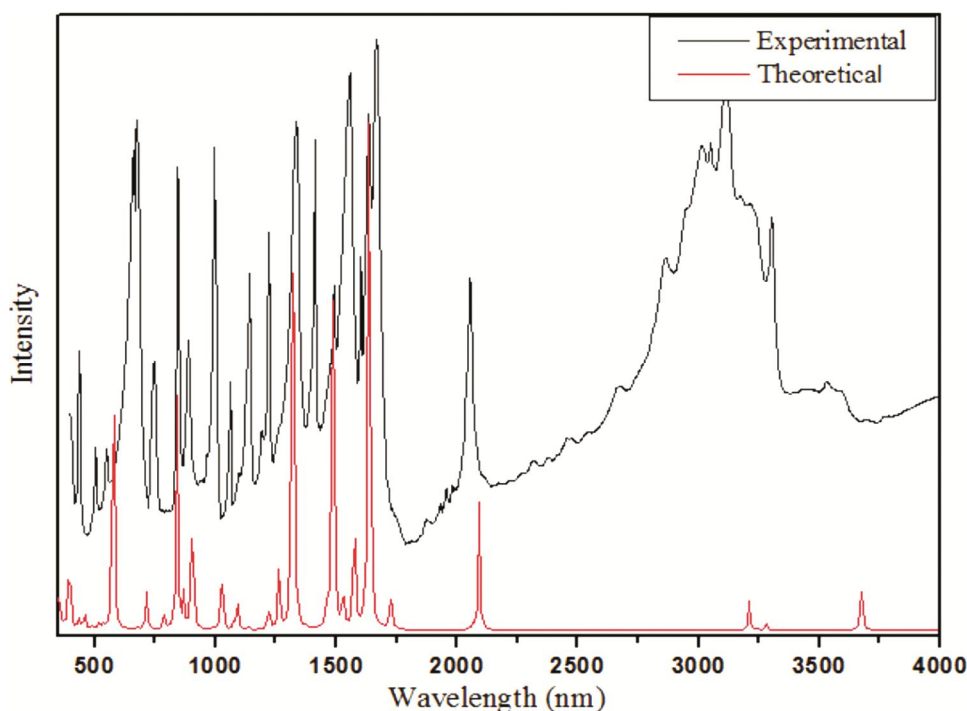

Fig. 4 – Comparisons between experimental and theoretical FT-IR spectra of the complex.

3.1.1 C=O vibrations

In aromatic compound, as a result of stretching motion of C=O group, a strong band appears in the FT-IR spectrum between 1690-1800 cm^{-1}, which indicates the presence of a carbonyl group[31]. The observed stretching vibration of carbonyl group appears at 1635.64 cm^{-1} whereas it is calculated at 1568.98 cm^{-1} in FT-IR spectrum which shows the good agreement with the experimental value.

3.1.2 C=C vibrations

In aromatic hydrocarbon[32], the C=C stretching vibration with in ring are observed in the region between 1600 to 1585 cm^{-1} and 1500 to 1400 cm^{-1}. The stretching vibration calculated at 1517.10 cm^{-1} assigned to the stretching vibration of C=C in the benzene ring which shows good agreement with experimental value at 1556.55 cm^{-1}.

3.1.3 NH₂ group vibrations

Molecule containing NH$_2$ group mainly shows absorption in the region between 3500-3220 cm^{-1}. The absorption position of NH$_2$ stretching vibration depends upon the degree of hydrogen bonding and the physical state of the sample or the polarity of the solvent[33]. In literature, it is reported that in case of a primary amine, a strong band represented in region of 3300-3450 cm^{-1}, shows asymmetrical N-H stretching modes while a weak band shown in between 3150-3270 cm^{-1}, represents symmetrical N-H stretching modes[34,35] and the bending vibrations are represented in the region 1580-1640 cm^{-1}. The NH$_2$ group

asymmetric and symmetric stretching vibrations for the given complex are observed at 3111.18 cm^{-1} and 3049.46 cm^{-1}, respectively, whereas their calculated vibrations are present, respectively, at 3436.78 and 3168.71 cm^{-1}.

3.1.4 CN group vibrations

CN group shows an intense absorption band in the region between (2280–2200) cm^{-1}. In the IR spectrum of given complex, the cyanide group stretching mode is observed at 2054.19 cm^{-1} while the calculated value for this mode is represented at 2001.34 cm^{-1}.

3.1.5 =C-H vibrations

Due to aromatic C-H stretching vibrations, the region normally lying between 3100 and 3000 cm^{-1} represents aromatic =C-H stretching modes[36]. The wavenumber calculated for =C-H stretching vibration is found at 3082.24 cm^{-1} while in FT-IR spectrum, a strong band observed at 3014.74 cm^{-1} is assigned for =C-H stretching vibration.

3.2 ^{1}H NMR and ^{13}C NMR spectroscopy

^{1}H NMR and ^{13}C NMR chemical shifts have been calculated, by using basis set DFT/B3LYP/LanL2DZ and applying GIAO approach. The experimental and calculated chemical shift values of ^{1}H NMR and ^{13}C NMR of synthesized complex have been given in Table 2 and Table 3, respectively, and their respective experimental ^{1}H NMR and ^{13}C NMR spectra are given in Fig. 5 and Fig. 6. The experimental values for H5 and H10 protons appear at 8.620 ppm and 7.639 ppm while the calculated values are obtained at 9.025 ppm and 7.099 ppm, respectively, and this is due to the de-shielding effect of nitrogen atom of pyridine ring. As D$_2$O is the solvent used in spectroscopy which leads to the rapid exchange of NH and NH$_2$ protons[37] with deuterium thus it diminish the peaks of NH(H23) and NH$_2$(H25 and H26) protons in the experimental spectral data of ^{1}H NMR. In ^{13}C NMR spectrum, experimental value at 167.06 ppm shows the presence of a (C=O) signal as comparable to the calculated value at 201.393 ppm. The difference in experimental values of C2, C3 and C4, C6 carbons is due to the de-shielding effect of nitrogen atom of pyridine ring, connected directly with C2 and C3 atoms. Carbon atoms of CN group(C11, C13, C15,C17 and C19) show a very sharp peak at 121.58 ppm which is overlapped with the peak of C4 and C6 carbons in spectrum hence it is shown as a very sharp peak.

3.3 Mass spectral analysis

The proposed molecular structure shows good agreement with the mass spectrum of the ruthenium (II)-isoniazid complex (Fig. 7). The presence of molecular ion peak, [M+H] at m/z = 365.00, confirms the stoichiometry of the complex formed.

3.4 Natural bond orbital analysis

NBO analysis helps in the determination of hybridization, co-valence, hydrogen-bonding and van der Waals interaction as it provides a useful way of information about interactions in both filled and virtual orbital spaces that helps in the interpretation of intra and intermolecular interactions. NBO analysis provides most possible 'natural Lewis structure' as it highlights the individual bonds and lone pair energy which participate in a chemical process[38,39]. The use of second order Fock matrix is to evaluate the donor-acceptor interactions in NBO analysis[40]. For each donor (i) and acceptor (j) the stabilization energy $E(2)$ associated with the delocalization $i \rightarrow j$ is given as:

$$E(2) = \Delta E_{ij} = qi \frac{\left(F_{ij}\right)^2}{\left(E_j - E_i\right)} \qquad ...(1)$$

Table 2 – Calculated and experimental ^{1}H NMR chemical shifts (δ/ppm) of compound in D$_2$O – solvent at 25 °C.

Atom	δcalcd.	δexp.	Assignment
H 5	9.0257		Benzene ring proton nearer to heterocyclic nitrogen atom
H 7	9.1236	8.620	heterocyclic nitrogen atom
H 9	6.7243		
H10	7.0997	7.639	Benzene ring
H23	6.9611		
H25	1.6642		Due to D$_2$O exchangeable protons, peaks does not appear in the spectrum
H26	1.7048		does not appear in the spectrum

Table 3 – Calculated and experimental ^{13}C NMR chemical shifts (δ / ppm) of compound in D$_2$O-solvent at 25 °C.

Atom	δcalcd.	δexp.	Assignment
C 2	167.8244	149.43	Benzene ring
C 3	168.3367		
C 4	122.234	121.92	Benzene ring
C 6	121.4791		
C 8	129.4335	140.61	Benzene ring carbon attached with carbonyl group
C11	132.2942		
C13	132.2873		
C15	132.275	121.58	CN group
C17	132.2646		
C19	129.8738		
C21	201.3931	167.06	Carbonyl group
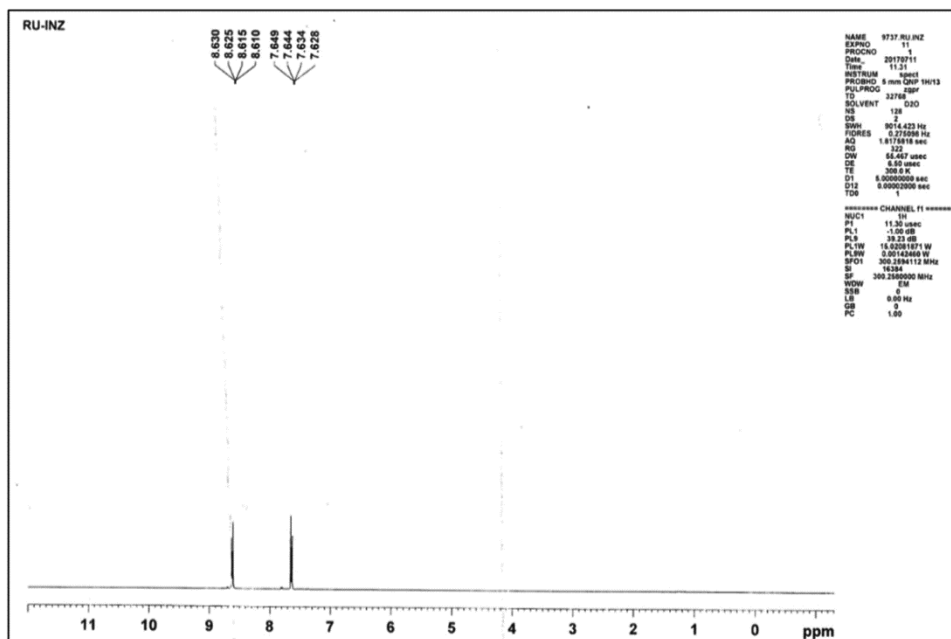
Fig. 5 – Experimental ^{1}H NMR spectrum of Ruthenium complex in D_2O solvent.
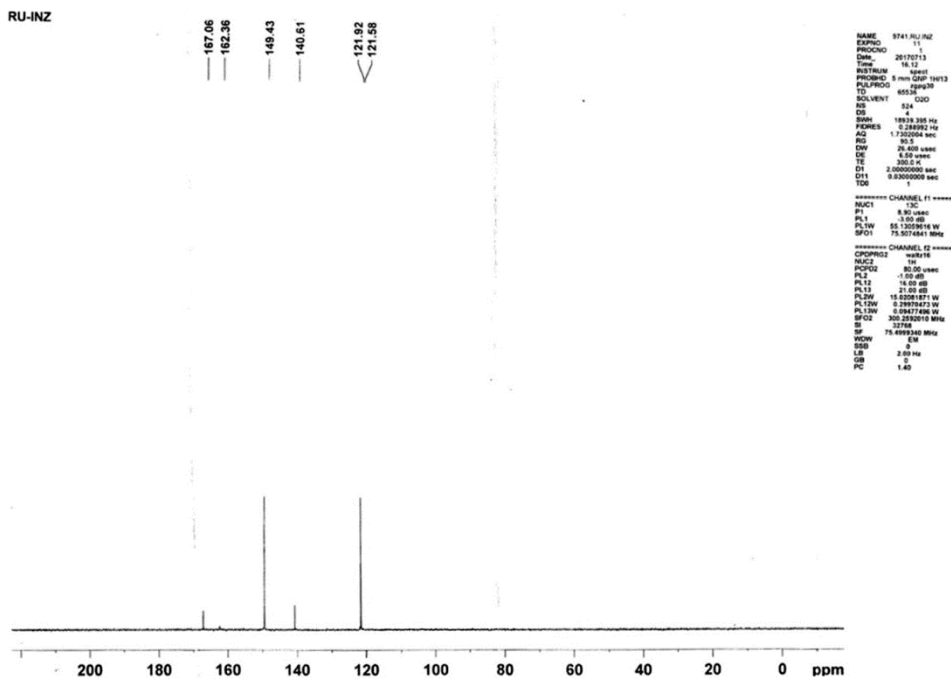
Fig. 6 – Experimental ^{13}C NMR spectrum of Ruthenium complex in D_2O solvent.

where q_i is the donor orbital occupancy, E_j and E_i are diagonal elements and F_{ij} is the off diagonal NBO Fock matrix element.

The higher value of $E(2)$ (stabilization energy or energy of hyperconjugative interaction) depicts greater interaction between electron donors and electron acceptors as the donating capacity from electron donors to electron acceptors increases, the extent of conjugation in the system increases[41]. A stabilized donor-acceptor interaction results from the delocalization of electron density between occupied Lewis-type (bonding or lone pair) NBO's and unoccupied (antibonding or Rydberg) non-Lewis NBO's. NBO analysis is carried out in the given
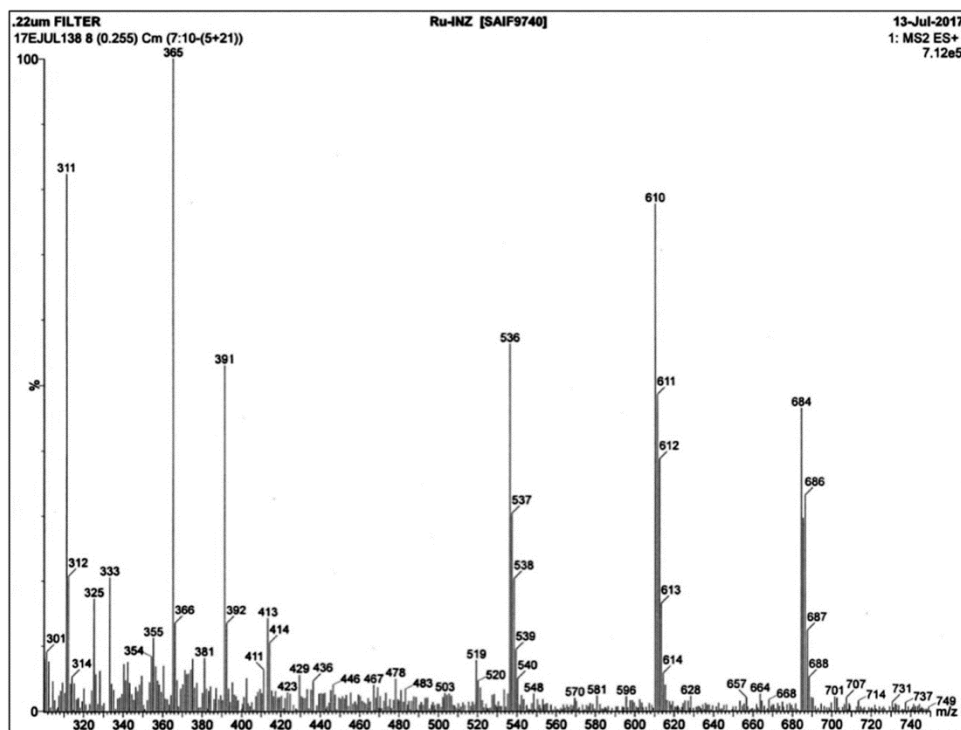
Fig. 7 – Experimental mass spectrum of the complex.

complex at the DFT/B3LYP/LanL2DZ level in order to determine the intra-molecular delocalization of electron density within the molecule. The possible intensive interactions have been given in Table 4. The following strong intra-molecular hyperconjugative interactions were observed which lead to the stabilization of the system, producing increased electron density (ED) and intramolecular charge transfer (ICT).

(i) From π(C19–N20) to π*(Ru1–N28) orbital with stabilization energy of 3.19 kcal/mol.

(ii) Fromσ (H23–N27) to π*(C21–O22) orbital with stabilization energy of 3.79 kcal/mol.

(iii) From n_2(O22) to σ*(C21–N27) orbital with stabilization energy of 34.65 kcal/mol.

(iv) From n_1(N24) to σ*(H23–N27) orbital with stabilization energy of 2.57 kcal/mol.

(v) From n_1(N27) to π*(C21–O22) orbital with stabilization energy of 9.21 kcal/mol.

3.5 Nonlinear optical properties

NLO effect is the extensively studied area of interest due to its immense applications in optical switching, optical modulation, frequency shifting, optical logic and optical memory for the emerging technologies in field of telecommunications, optical interconnections and signal processing[42-44]. For comparative purpose, urea is used as a threshold value since most of the nonlinear optical (NLO) properties of molecular systems are studied using urea. The use of density functional theory is in calculating the dipole moment (μ), mean polarizability (α) and the total first static hyperpolarizability (β_o) of the compound in terms of x, y and z components. The calculations were performed using DFT/B3LYP/LanL2DZ basis set. It is known that NLO property increases with increase in dipole moment, molecular polarizability and first order hyperpolarizability of the system. The complete equations to calculate the magnitude of the total static dipole moment (μ), the isotropic polarizability (α_o), anisotropy of the polarizability ($\Delta\alpha$) and the first order hyperpolarizability (β_o) using the x, y and z component are given as:

$$\mu_{tot} = (\mu_x^2 + \mu_y^2 + \mu_z^2)^{1/2} \qquad \ldots(2)$$

$$\alpha_{tot} = 1/3\ (\alpha_{xx} + \alpha_{yy} + \alpha_{zz}) \qquad \ldots (3)$$

$$\beta = [(\beta_{xxx} + \beta_{xyy} + \beta_{xzz})^2 + (\beta_{yyy} + \beta_{yzz} + \beta_{yxx})^2 + (\beta_{zzz} + \beta_{zxx} + \beta_{zyy})^2]^{1/2} \qquad \ldots(4)$$

The values of calculated dipole moment and hyperpolarizability have been shown in Table 5. The value of the polarizabilities (α) and the hyperpolarizabilities are given in atomic units (a.u.), so they have been converted in to electronic units

Table 4 – Second–order perturbation theory analysis of the Fock matrix in NBO basis for (**3**): Selected donor (Lewis) and acceptor (non–Lewis) orbitals, percentage electron density over bonded atoms (ED_A, ED_B in%), NBO hybrid orbitals of bonded atoms and stabilization energy of various intra-molecular interactions $E(2)$.

Donor (i)			Acceptor (j)			$E(2)$ (kcal/mol)
Orbital / lp (occupancy)	ED_A, % ED_B, %	NBO hybrid orbitals	orbital (occupancy)	ED_A, % ED_B, %	NBO hybrid orbitals	
σ (Ru1-C11) (1.88026)	33.17 66.83	$0.576(sp^{2.79})_{Ru}$ $0.8175(sp^{0.63})_C$	σ*(Ru1-C13) (0.10853)	66.79 33.21	$0.8173(sp^{2.79})_{Ru}$ $-0.5763(sp^{0.63})_C$	8.40
σ (Ru1-C13) (1.87993)	33.21 66.79	$0.576(sp^{2.79})_{Ru}$ $0.8173(sp^{0.63})_C$	σ*(Ru1-C11) (0.10851)	66.83 33.17	$0.8175(sp^{2.79})_{Ru}$ $-0.5759(sp^{0.63})_C$	8.42
σ (Ru1–C15) (1.87963)	33.25 66.75	$0.576(sp^{2.79})_{Ru}$ $0.8170(sp^{0.64})_C$	σ*(Ru1-C17) (0.10854)	66.78 33.22	$0.8172(sp^{2.79})_{Ru}$ $-0.5764(sp^{0.64})_C$	8.47
σ (Ru1-C17) (1.87982)	33.22 66.78	$0.576(sp^{2.79})_{Ru}$ $0.8172(sp^{0.64})_C$	σ*(Ru1-C15) (0.10849)	66.75 33.25	$0.8170(sp^{2.79})_{Ru}$ $-0.5766(sp^{0.64})_C$	8.46
σ (Ru1–C19) (1.84380)	33.92 66.08	$0.582(sp^{3.31})_{Ru}$ $0.8129(sp^{0.67})_C$	σ*(Ru1–N28) (0.17337)	83.12 16.88	$0.9117(sp^{3.74})_{Ru}$ $-0.4108(sp^{1.66})_N$	17.03
σ (Ru1–N28) (1.89014)	16.88 83.12	$0.410(sp^{3.74})_{Ru}$ $0.912(sp^{1.66})_N$	σ*(Ru1–C19) (0.10089)	66.08 33.92	$0.8129(sp^{3.31})_{Ru}$ $-0.5824(sp^{0.67})_C$	11.47
π (Ru1–N28) (1.83962)	61.22 38.78	$0.782(sp^{1.00})_{Ru}$ $0.623(sp^{1.00})_N$	π*(C2–C4) (0.25930)	53.20 46.80	$0.7294(sp^{1.00})_C$ $-0.6841(sp^{1.00})_C$	16.30
σ (C2–C4) (1.97913)	48.51 51.49	$0.6965(sp^{1.71})_C$ $0.7175(sp^{1.77})_C$	σ*(C8–C21) (0.05996)	49.51 50.49	$0.7036(sp^{2.59})_C$ $-0.7106(sp^{1.46})_C$	5.02
σ (C2–H5) (1.97175)	62.43 37.57	$0.7901(sp^{2.01})_C$ $0.6130(sp^{0.00})_H$	σ*(C3–N28) (0.02963)	62.59 37.41	$0.7911(sp^{2.34})_C$ $-0.6117(sp^{2.21})_H$	6.15
σ (C2–N28) (1.97909)	37.53 62.47	$0.6126(sp^{2.33})_c$ $0.7904(sp^{2.22})_N$	σ*(Ru1–N28) (0.17337)	83.12 16.88	$0.9117(sp^{3.74})_{Ru}$ $-0.4108(sp^{1.66})_N$	7.44
σ (C3–C6) (1.97786)	48.68 51.32	$0.6977(sp^{1.71})_C$ $0.7164(sp^{1.78})_C$	σ*(C8–C21) (0.05996)	49.51 50.49	$0.7036(sp^{2.59})_C$ $-0.7109(sp^{1.46})_C$	5.51
σ (C3–H7) (1.97106)	62.52 37.48	$0.7907(sp^{2.00})_C$ $0.6122(sp^{0.00})_H$	σ*(C2–N28) (0.02911)	62.47 37.53	$0.7904(sp^{2.33})_C$ $-0.6126(sp^{2.22})_N$	6.21
σ (C3–N28) (1.97949)	37.41 62.59	$0.6117(sp^{2.34})_C$ $0.7911(sp^{2.21})_N$	σ*(Ru1–N28) (0.17337)	83.12 16.88	$0.9117(sp^{3.74})_{Ru}$ $-0.4108(sp^{1.66})_N$	7.49
σ (C4–H9) (1.97476)	59.98 40.02	$0.7745(sp^{2.56})_C$ $0.6326(sp^{0.00})_H$	σ*(C6–C8) (0.02342)	51.00 49.00	$0.7141(sp^{1.81})_C$ $-0.7000(sp^{1.72})_C$	5.91
σ (C6–H10) (1.97429)	61.20 38.80	$0.7823(sp^{2.51})_C$ $0.6229(sp^{0.00})_H$	σ*(C4–C8) (0.02512)	50.53 49.47	$0.7109(sp^{1.79})_C$ $-0.7033(sp^{1.82})_C$	6.16
σ (C8–C21) (1.97194)	50.49 49.51	$0.7106(sp^{2.59})_C$ $0.7036(sp^{1.46})_C$	σ*(C2–C4) (0.02077)	51.49 48.51	$0.7175(sp^{1.71})_C$ $-0.6965(sp^{1.77})_C$	3.91
π(C19–N20) (1.97099)	40.10 59.90	$0.6332(sp^{1.00})_C$ $0.7740(sp^{1.00})_N$	π*(Ru1–N28) (0.85210)	38.78 61.22	$0.6227(sp^{1.00})_{Ru}$ $-0.7825(sp^{1.00})_N$	3.19
σ(H23–N27) (1.97446)	30.90 69.10	$0.5559(sp^{0.00})_H$ $0.8313(sp^{3.81})_N$	π*(C21–O22) (0.33128)	69.13 30.87	$0.8314(sp^{89.16})_C$ $-0.5556(sp^{98.94})_O$	3.79
n_2(O22) (1.85814)	-	$(sp^{99.99})_O$	σ*(C21–N27) (0.12554)	64.00 36.00	$0.8000(sp^{2.60})_C$ $-0.6000(sp^{2.27})_N$	34.65
n_1(N24) (1.97541)	-	$(sp^{3.70})_N$	σ*(H23–N27) (0.02412)	69.10 30.90	$0.8313(sp^{0.00})_H$ $-0.5559(sp^{3.81})_N$	2.57
n_1(N27) (1.90634)	-	$(sp^{2.85})_N$	π*(C21–O22) (0.33128)	69.13 30.87	$0.8314(sp^{89.16})_C$ $-0.5556(sp^{98.94})_O$	9.21

Table 5 – Calculated dipole moment (μ_0), polarizability ($|\alpha_0|$), anisotropy of polarizability ($\Delta\alpha$), first hyperpolarizability (β_0) and their components, using B3LYP/LanL2DZ (in water).

Dipole moment		Polarizability		Hyperpolarizability	
μx	23.5798	Axx	516.693	Bxxx	8772.39
μy	-2.5089	Ayy	10.882	Bxxy	428.989
μz	1.6693	Azz	197.979	Bxyy	-132.88
μ	23.7715	Axy	-0.1909	Byyy	-31.786
		Axz	-1.2411	Bxxz	121.055
		Ayz	159.454	Bxyz	-25.263
		$\alpha 0$	35.8424	Byyz	20.1313
		$\Delta\alpha$	147.987	Bxzz	37.9027
				Byzz	-28.67
				Bzzz	10.2122
				$\beta 0$	75.0458

μ_0 in Debye; $|\alpha_0|$ and $\Delta\alpha$ in 10^{-24}esu; β_0 in 10^{-30}esu,

(e.s.u.) (for α: 1a.u = 0.1482×10^{-24} esu and for β: 1a.u = $0.0086393 \times 10^{-30}$esu). The total molecular dipole moment of given compound is 23.7715 D which is seventeen times greater than the dipole moment of urea (μ of urea = 1.3732 Debye). The calculated first hyperpolarizability is 75.0458×10^{-30}esu which is two hundred one times greater than the hyperpolarizability of urea (β of urea = 0.3728×10^{-30} esu).

3.6 Thermodynamic properties

Thermodynamic properties are used in various chemical and physical processes. Some thermodynamic parameters of synthesized complex, including zero-point vibrational energy, rotational temperatures, rotational constants, energies were evaluated at standard temperature 298.15 K (in gas phase) and their values were obtained using DFT/B3LYP/CAM-B3LYP functional with LanL2DZ basis set and are listed in Table 6. The standard statistical thermodynamic functions such as heat capacity (CV), entropy (S) were obtained at different temperatures (from 100 K to 600 K) on the basis of vibrational analysis, using DFT/B3LYP/LanL2DZ basis set (Table 7). The values of rotational constants and rotational temperatures are found to be similar in almost all the cases. It is found that as temperature increase from 100 K to 600 K, the standard statistical thermodynamic functions also increase with temperature and this is due to the fact that molecular vibrational intensities increase with temperature[45,46].

The correlation equations among heat capacities, entropies and temperatures were fitted by quadratic formulas and the corresponding fitting factors (R^2) for these thermodynamic properties are given in following Eqs (5), (6), (7) and (8). The corresponding

Table 6 – Calculated thermodynamic parameters of $[Ru(CN)_5INH]^{3-}$ complex.

Parameters	B3LYP LanL2DZ
Zero point Vibrational Energy (kcal/mol)	109.080
Rotational Temperature (K)	0.02543
	0.00647
	0.00625
Rotational Constant (GHz)	
X	0.52988
Y	0.13484
Z	0.13016
Total Energy E_{total} (kcal/mol)	123.666
Translational	0.889
Rotational	0.889
Vibrational	121.889

Table 7 – Thermodynamic functions at different temperatures at the B3LYP and CAM-B3LYP/LanL2DZ level

Temperature (T) (K)	Heat capacity (CV) (Cal/mol K)		Entropy (S) (Cal/mol K)	
	B3LYP LanL2DZ	CAM-B3LYP LanL2DZ	B3LYP LanL2DZ	CAM-B3LYP LanL2DZ
100	19.749	21.943	76.721	80.581
200	40.591	42.963	98.468	103.876
300	56.224	58.915	118.830	125.262
400	68.444	71.389	137.317	144.560
500	78.206	81.339	154.122	162.043
600	86.103	89.373	169.465	177.970

fitting equations are given below and their respective correlation graphics are shown in Fig. 8 and Fig. 9.

$$CV = -2.1655 + 0.2408T - 2.10^{-4}T^2 \quad (R^2 = 0.9993)$$
$$\text{using B3LYP} \quad \text{...(5)}$$

$$S = 53.196 + 0.2433T - 5.10^{-8}T^2 \ (R^2 = 1)$$
$$\text{using B3LYP} \quad \text{... (6)}$$

$$CV = 0.3112 + 0.244T - 2.10^{-4}T^2 \ (R^2 = 0.9994)$$
$$\text{using CAM-B3LYP} \quad \text{... (7)}$$

$$S = 55.566 + 0.2601T - 5.10^{-9}T^2 \ (R^2 = 1)$$
$$\text{using CAM- B3LYP} \quad \text{... (8)}$$

These thermodynamic data plays an important role in further study of the synthesized complex such as in computation of other thermodynamic energies according to the relationship of thermodynamic functions and in estimation of direction of chemical reactions according to the second law of thermodynamics in thermo chemical field[47].

3.7 Global reactivity descriptors

Koopman's theorem provides the basis for the determination of chemical reactivity and site

selectivity of molecular systems. Energies of frontier molecular orbital (ε_{HOMO}, ε_{LUMO}), band gap ($\varepsilon_{LUMO} - \varepsilon_{HOMO}$), ionization potential (IP), electron affinity (EA), electronegativity (χ), global hardness (η), chemical potential (μ), global electrophilicity index (ω) and global softness (S) are global reactivity descriptors, help in prediction of global reactivity trends. These global reactivity descriptors have been evaluated through given equations[48-52].

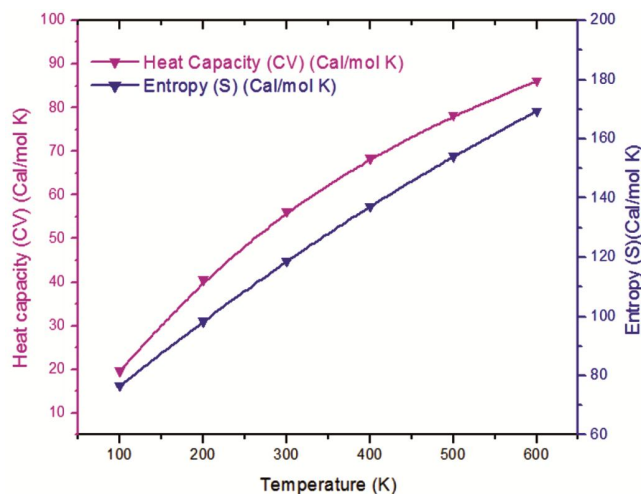$$IP = -\varepsilon_{HOMO} \qquad \ldots (9)$$

Fig. 8 – Correlation graphs of heat capacity and entropy calculated at various temperatures using B3LYP.
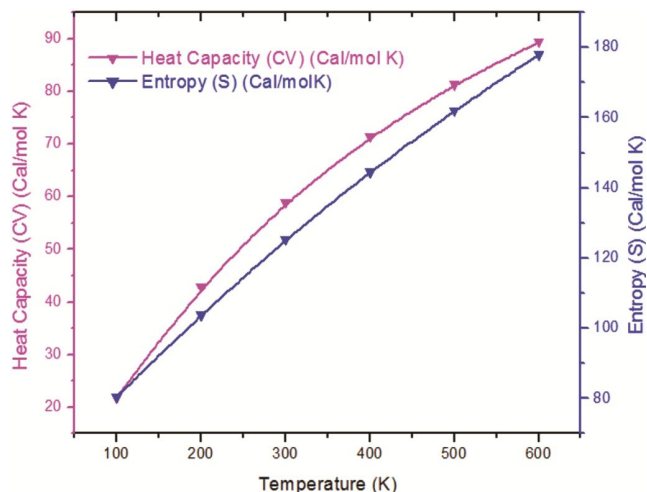
Fig. 9 – Correlation graphs of heat capacity and entropy calculated at various temperatures using CAM-B3LYP.

$$EA = -\varepsilon_{LUMO} \qquad \ldots (10)$$

$$\chi = -\frac{1}{2}\left(\varepsilon_{LUMO} + \varepsilon_{HOMO}\right) \qquad \ldots (11)$$

$$\eta = \frac{1}{2}\left(\varepsilon_{LUMO} - \varepsilon_{HOMO}\right) \qquad \ldots (12)$$

$$\mu = -\chi = \frac{1}{2}\left(\varepsilon_{LUMO} + \varepsilon_{HOMO}\right) \qquad \ldots (13)$$

$$\omega = \frac{\mu^2}{2\eta} \qquad \ldots (14)$$

$$S = \frac{1}{2\eta} \qquad \ldots (15)$$

These above mentioned parameters were calculated for product, using the energies of frontier molecular orbitals (ε_{LUMO}, ε_{HOMO}) and are tabulated in Table 8.

According to Parr *et al.*, electrophilicity index (ω) is a positive and definite quantity. This is a global reactivity index and similar to the chemical hardness and chemical potential. Stabilization in energy has been measured by this new reactivity index as the system acquires an additional electronic charge (ΔN) from the environment. Electronic chemical potential of the molecule helps in the determination of direction of charge transfer because as electrophile accepts electronic charge its energy must decrease so its chemical potential must be negative. Various types of reactions and their most reactive positions in conjugated system are mostly described with the help of molecular orbital and their properties such as energy[53]. In a molecule, HOMO (Highest occupied molecular orbital) and LUMO (Lowest unoccupied molecular orbital) play a major role as their values and their energy gap represents the biological activity of the molecule. HOMO, as an electron donor, tends to give its outer orbital containing electrons, hence its energy is directly related with the ionization potential. While the LUMO can acquire electrons and electron affinity is directly related with the energy of LUMO[54,55]. Small frontier orbital gap generally depicts more polarizability of a molecule with high chemical reactivity and low kinetic stability[56-58].

Table 8 – Calculated ε_{LUMO}, ε_{HOMO}, energy band gap $\varepsilon_{LUMO} - \varepsilon_{HOMO}$, ionization potential (IP), electron affinity (EA), electronegativity (χ), global hardness (η), chemical potential (μ), global electrophilicity index (ω) and global softness (S) in eV for ruthenium-isoniazid complex, using B3LYP/LanL2DZ basis set..

	ε_H	ε_L	ε_L-ε_H	I	A	x	n	μ	ω	S
Complex Ru-INH	-0.177	-0.076	-0.101	0.177	0.076	0.126	0.051	-0.126	0.156	9.80

In the given compound this transition appears due to $n \rightarrow \pi^*$ transition. This electronic transition corresponds to the transition from HOMO molecular orbital to LUMO molecular orbital as shown in Fig. 10 with energy levels of HOMO and LUMO orbital at B3LYP/LanL2DZ level. The HOMO and LUMO orbitals are separated with an energy gap of 2.4672 eV.

3.8 Mulliken atomic charges analysis

The Mulliken atomic charge is one of the important factors that is directly linked with the vibrational characteristics of the molecule. It shows the nature of chemical bond in a molecular system. This factor helps us to explain the electronegativity equalization and charge transfer processes during a chemical reaction. This factor influences several molecular properties such as electronic structure, dipole moment and polarizability[59]. It also helps us to depict the changes in electronic structure during atomic displacement[60]. The net atomic charges which are obtained by Mulliken population analysis of $[Ru(CN)_5INH]^{3-}$ complex are given in Table 9 and shown in Fig. 11 and its corresponding

Mulliken plot with basis set B3LYP/LanL2DZ is shown in Fig. 12.

The charge distribution of $[Ru(CN)_5INH]^{3-}$ complex represented that the C(2), C(3), C(4) and C(6) carbon atoms are attached with hydrogen atoms, are negative in values, whereas C(21) carbon atom which is attached with electronegative atoms (oxygen and nitrogen) is positively charged since these electronegative atoms withdraw partial charges from the carbon atom and makes C(21) carbon atom positive in value except C(11), C(13), C(15) and C(17) carbon atoms which show negative values, being attached with nitrogen atoms and it may be due to the greater electropositive character of Ru(1) atom. Similarly C(8) carbon atom shows positive value due to the electronegative effect of oxygen and nitrogen atoms, present at alternate position. All the hydrogen atoms show net positive charge. The high negative charge on N(12), N(14), N(16), N(18), N(20), N(24), N(27),N(28) and O(22) atoms are due to their electron withdrawing nature.
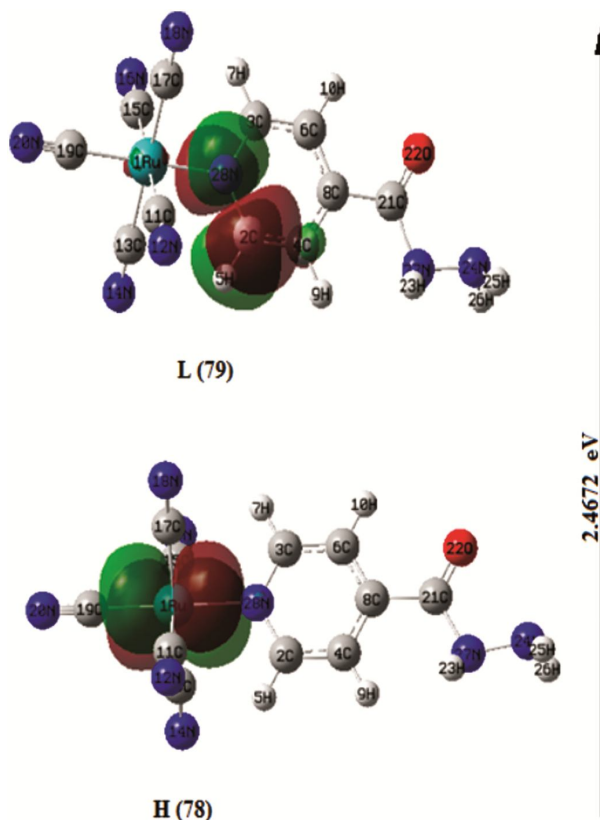

Fig. 10 – Molecular orbitals (HOMO → LUMO) of the complex at the B3LYP/LanL2DZ basis set.

Table 9 – Mulliken atomic charges distribution of $[Ru(CN)_5INH]^{3-}$ complex, performed at B3LYP/ LanL2DZ basis set.

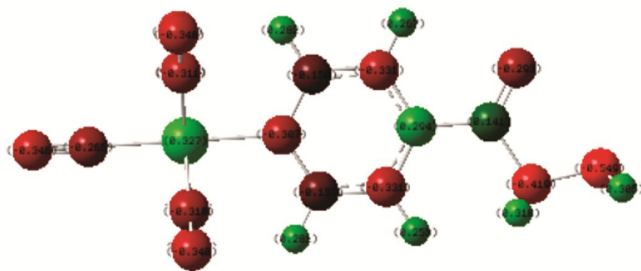| Atoms	Mulliken atomic charges
Ru_1	0.550764
C_2	-0.111242
C_3	-0.102066
C_4	-0.341576
H_5	0.297402
C_6	-0.326356
H_7	0.300708
C_8	0.292721
H_9	0.213854
H_{10}	0.248569
C_{11}	-0.253324
N_{12}	-0.260210
C_{13}	-0.253457
N_{14}	-0.257971
C_{15}	-0.253605
N_{16}	-0.255739
C_{17}	-0.254032
N_{18}	-0.256711
C_{19}	-0.164303
N_{20}	-0.231318
C_{21}	0.129116
O_{22}	-0.250766
H_{23}	0.262719
N_{24}	-0.501783
H_{25}	0.251764
H_{26}	0.282452
N_{27}	-0.407350
N_{28}	-0.348260

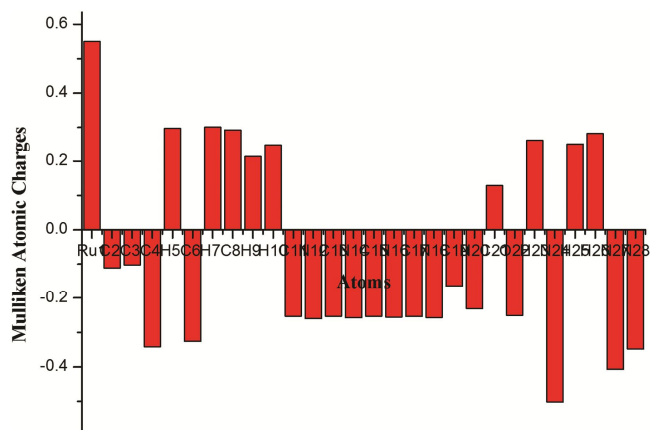Fig. 11 – Mulliken charge distribution per atom in $[Ru(CN)_5INH]^{3-}$ complex.

Fig. 12 – Mulliken plot of $[Ru(CN)_5INH]^{3-}$ complex.

4 Conclusions

The present work describes efficient synthetic route for the preparation of the complex $[Ru(CN)_5INH]^{3-}$. The identity and the structural integrity of the synthesized complex have been confirmed by UV spectroscopy, IR spectroscopy, NMR spectroscopy, C13 spectroscopy, mass spectroscopy and elemental analysis. For the given complex we have calculated vibrational frequencies, Mulliken charges, NBO properties, NLO properties, ^1H NMR and ^{13}C NMR chemical shifts theoretically as well as experimentally. ^1H NMR and ^{13}C NMR chemical shift values were obtained by GIAO method shows good agreement with the experimental values. NBO analysis reveals the charge transfer within the molecule. The calculated first order hyperpolarizability of the given complex is 75.0458×10^{-30} esu which is greater than the standard NLO material urea (β of urea = 0.3728×10^{-30} esu) which shows that the given complex may be useful as a nonlinear optical material.

Acknowledgement

References

1 World Health Organization (WHO), Tuberculosis fact sheet No. 104-*global andregional incidence,* March, 2006.
2 Sriram D, Yogeeswari P & Madhu K, *Bioorg Med Chem Lett*, 15 (2005) 4502.
3 Rickman K A, Swancutt K L, Mezyk S P & Kiddle J J, *Bioorg Med Chem Lett*, 23 (2013) 3096.
4 Dandawate P, Vemuri K, Swamy K V, Khan E M, Sritharan M & Padhye S, *Bioorg Med Chem Lett*, 24 (2014) 5070.
5 World Health Organization (WHO) Report, *Global Tuberculosis Controls,* Geneva, Switzerland, 2003.
6 Naik R M, Prasad S, Kumar B, Yadav S B S, Asthana A & Yoshida M, *Microchem J*, 111 (2013) 108.
7 Bax H I, Bakker-Woudenberg I A J M, deVogel C P, Van der Meijden A, Verbon A & de Steenwinkle J E M, *Tuberculosis*, 105 (2017) 80.
8 World Health Organization (WHO), *Tuberculosis global facts,* (Accessed April 05, 2012), 2010.
9 Korokovals A, *Essentials of medicinal chemistry*, 2nd Edn (Wiley-Interscience: New York), 1998.
10 Meyer H & Mally J, *Monatshefte*, 33 (1912) 393.
11 Lock G, *Pharm Ind*, 14 (1952) 366.
12 Argyrou A, Vetting M W, Aladegbami B & Blanchard J S, *Nat Struct Mol Biol*, 13 (2006) 408.
13 ZhangY, Heym B, Allen B, Young D & Cole S, *Nature*, 358 (1992) 3.
14 Khuhawar M Y & Zardari L A, *J Food Drug Anal*, 14 (2006) 323.
15 Brossier F & Sougakoff W, *Med Mal Infect*, 47 (2017) 340.
16 Santos E R, Mondelli M A, Pozzi L V, Correa R S, Salistre-de-Araujo H S, Pavan F R, Leite C Q F, Ellena J, Malta V R S, Machado S P & Batista A A, *Polyhedron*, 51 (2013) 292.
17 Sousa E H S, Basso L A, Santos D S, Diogenes I C N, Longhinotti E, Lopes L G D & Moreira I D S, *J Biol Inorg Chem*, 17 (2012) 275.
18 Bergamo A, Gaiddon C, Schellens J H M, Beijnen J H & Sava G, *J Inorg Biochem*, 106 (2012) 90.
19 De Oliveira R S, Boffo E F, Reis F C C, Nikolaou S, Andriani K F, Caramori G F & Doro F G, *Polyhedron*, 114 (2016) 232.
20 Ramachandran R, Prakash G, Nirmala M, Viswanathamurthi P & Malecki J G, *J Organomet Chem*, 791 (2015) 130.
21 Naik RM, Singh R & Asthana A, *Int J Chem Kinet*, 43 (2011) 21.
22 Baran Y, *Transition Met Chem*, 25 (2000) 41.
23 Johnson C R & Shepherd R E, *Inorg Chem*, 22 (1983) 1117.
24 Punnarao A B, Gulati K, Joshi N, Deb D K, Rambabu D, Kaminsky W, Poluri K M & Kollipara M R, *Inorg Chim Acta*,1693 (2017) 7-30488.
25 Konstantinov I A & Broadbelt L J, *J Phys Chem A*, 115 (2011) 12364.
26 Merrick J P, Moran D & Radom L, *J Phys Chem A*, 111 (2007) 11683.
27 BaroneV, Cossi M & Thomasi J, *J ComputChem*, 19 (1998) 404.

28 Weinhold F & Landis C R, *Valency and bonding: A natural bond orbital donor- acceptor perspective*, (Cambridge University Press, Cambridge: New York), 2005.

29 Frisch M J, Trucks G W, Schlegel H B, Scuseria G E, Robb M A, Cheeseman J R, Scalmani G, Barone V, Mennucci B, Petersson G A, Nakatsuji H, Caricato M, Li X, Hratchian H P, Izmaylov A F, Bloino J, Zheng G, Sonnenberg J L, Hada M, Ehara M, Toyota K, Fukuda R, Hasegawa J, Ishida M, Nakajima T, Honda Y, Kitao O, Nakai H, Vreven T, Montgomery J A, Peralta J E, Ogliaro F, Bearpark M, Heyd J J, Brothers E, Kudin K N, Staroverov V N, Keith T, Kobayashi R, Normand J, Raghavachari K, Rendell A, Burant J C, Iyengar S S, Tomasi J, Cossi M, Rega N, Millam J M, Klene M, Knox J E, Cross J B, Bakken V, Adamo C, Jaramillo J, Gomperts R, Stratmann R E, Yazyev O, Austin A J, Cammi R, Pomelli C, Ochterski J W, Martin R L, Morokuma K, Zakrzewski V G, Voth G A, Salvador P, Dannenberg J J, Dapprich S, Daniels A D, Farkas O, Foresman J B, Ortiz J V, Cioslowski J, & Fox D J, *Gaussian 09, Revision B.01,* (Gaussian, Inc: Wallingford CT), 2010.

30 Yoshida H, Ehara A & Matsuura H, *Chem Phys Lett*, 325 (2000) 477.

31 Karabacak M & Kurt M, *J Mol Struct*, 919 (2009) 215.

32 Krishnakumar V, Manohar S & Nagalakshmi R, *Spectrochim Acta A*, 71 (2008) 110.

33 Gunasekaran S, Kumaresan S, Balaji R A, Anand G & Seshadri S, *J Phys*,71 (2008) 1291.

34 Silverstein R M, Webster F X, *Spectrometric identification of organic compounds*, 6th Edn, (John Wiley & Sons: New York), 1963.

35 Roeges N P G, *A Guide to the complete interpretation of infrared spectra of organic structures*, (Wiley: New York), 1994.

36 Varsanyi G, *Vibrational spectra of benzene derivatives*, (Academic Press: New York), 1969.

37 Shrivastava M, Sharma M & Koty A, *Oriental J Chem*, 28 (2012)1711.

38 Guo D & Goodman L, *J Phys Chem*, 100 (1996) 12540.

39 Weinhold F, *Nature*, 411 (2001) 539.

40 Foster J P & Weinhold F, *J Am Chem Soc*, 102 (1980) 7211.

41 Liu C G, Su Z M, Guan X H & Muhammad S, *J Phys Chem C*, 115 (2011) 23946.

42 Andraud C, Brotin T, Garcia C, Pelle F, Goldner P, Bigot B & Collet A, *J Am Chem Soc*, 116 (1994) 2094.

43 Nakano M, Fujita H, Takahata M & Yamaguchi K, *J Am Chem Soc*, 124 (2002) 9648.

44 Geskin V M, Lambert C & Bredas J L, *J Am Chem Soc*, 125 (2003) 15651.

45 Bevan O J, Boerio-Goates J, *Calculations from statistical thermodynamics*, (Academic Press), 2000.

46 Sajan D, Josepha L, Vijayan N & Karabacak M, *Spectrochim Acta A*, 81 (2011) 85.

47 Zhang R, Dub B, Sun G & Sun Y, *Spectrochim Acta A*, 75 (2010) 1115.

48 Pearson R G, *J Org Chem*, 54 (1989) 1430.

49 Parr R G & Pearson R G, *J Am Chem Soc*, 105 (1983) 7512.

50 Geerlings P, De P F & Langenaeker W, *Chem Rev*, 103 (2003) 1793.

51 Parr R G, Szentpály L & Liu S, *J Am Chem Soc*, 121 (1999) 1922.

52 Chattaraj P K, Sarkar U & Roy D R, *Chem Rev*, 106 (2006) 2065.

53 ChoudharyN, Bee S, Gupta A & Tandon P, *Comp Theor Chem*, 1016 (2013) 8.

54 Fukui K, *Science*, 218 (1982) 747.

55 Gece G, *Corros Sci*, 50 (2008) 2981.

56 Sinha L, Prasad O, Narayan V & Shukla S R, *J Mol Simul*, 37 (2011) 153.

57 Lewis D F V, Loannides C & Parke D V, *Xenobiotica*, 24 (1994) 401.

58 Kosar B & Albayrak C, *Spectrochim Acta A*, 78 (2011) 160.

59 Govindarajan M & Karabacak M, *Spectrochim Acta A*, 96 (2012) 421.

60 Guidara S, Ahmed A B, Abid Y & Feki H, *Spectrochim Acta A*, 127 (2014) 275.